The Influence of the Surface Character of the Clays on the Properties of Poly(*p*-dioxanone)/Fibrous Clay Nanocomposites

Zhi-Cheng Qiu, Jing-Jing Zhang, Cai-Li Huang, Ying Niu, Ke-Ke Yang, Yu-Zhong Wang

Center for Degradable and Flame-Retardant Polymeric Materials (ERCEPM-MoE), National Engineering Laboratory of Eco-Friendly Polymeric Materials (Sichuan), State Key Laboratory of Polymer Materials Engineering, College of Chemistry, Sichuan University, Chengdu 610064, People's Republic of China

Received 21 February 2011; accepted 2 June 2011
DOI 10.1002/app.35040
Published online 12 January 2012 in Wiley Online Library (wileyonlinelibrary.com).

ABSTRACT: Two different fibrous clays, halloysite nanotubes (HNTs) and organically modified attapulgite (OAT), were chosen to prepare poly(*p*-dioxanone) (PPDO)/clay nanocomposites by *in-situ* polymerization. The influence of surface character and geometric structure of the clays on the properties of the nanocomposites were investigated systematically concerning with their crystallization behaviors, thermal stabilities, rheological behaviors, and mechanical performances. The effect of clay content on the properties of the nanocomposites was also discussed, taking PPDO/HNTs nanocomposites for example. The results showed that HNTs was more effective in improving the crystallization rate, thermal stability as well as mechanical performance. In addition, the crystallization rate and rigidity of nanocomposites increased with increasing HNTs loading. © 2012 Wiley Periodicals, Inc. J Appl Polym Sci 125: E247–E259, 2012

Key words: poly(*p*-dioxanone); halloysite nanotubes; attapulgite; nanocomposites; surface character

INTRODUCTION

Poly(*p*-dioxanone) (PPDO) is biodegradable, bioabsorbent, and biocompatible thermoplastic polymer, which has been applied practically in the medical field.[1–8] As the cost of the monomer of PPDO has been reduced, it is possible for PPDO to be used as general material. However, its relatively slow crystallization rate and low melt strength have limited its further practical application. To overcome these disadvantages, copolymer synthesis,[1,9–11] polymer blending,[12–15] and reinforced composites methods[3,16–25] have been developed. Due to the nanoscale dispersion and the high surface-to-volume ratio, nanoparticles reinforced composites are regarded as a useful and convenient way to improve the performance of polymers.[26] In our previous work, we have prepared PPDO/montmorillonite (MMT) nanocomposites with intercalated structure.[16–17] These PPDO/MMT nanocomposites had remarkably increased crystallization rate and improved melt strength; moreover, they could be blown into thin films.

Carbon nanotubes (CNTs) have been considered as ideal reinforcing fillers in polymer nanocomposite with high performance, due to their high aspect ratio, nanosize in diameter, very low density, and excellent physical properties such as extremely high mechanical strength.[27,28] However, CNTs are so expensive, which limits its commercial application. It highlights the need to explore alternative nanofibers to enhance polymer properties. In this work, two kinds of silicate nanofibers, halloysite nanotubes (HNTs) and organically modified attapulgite (OAT), were introduced into PPDO matrix, respectively. Both of them are mined from natural deposits. HNTs, with hollow nanotubular structure, are a kind of aluminosilicate clays with $Al_2Si_2O_5(OH)_4{\cdot}2H_2O$ as the unit cell formula.[29] The outer surface of HNTs is composed of siloxane and most hydroxyls of HNTs are located in the inner surface, indicating that HNTs possess much better dispersion property than other natural clays such as MMT and attapulgite (AT).[30] The size of HNTs is 0.5–2 μm in length, 50–70 nm for the outer diameter, and 10–30 nm for the inner diameter. OAT is a kind of fibrous magnesium aluminum clays with $Mg_5Si_8O_{20}(OH_2)_2(OH)_4{\cdot}4H_2O$ as the unit cell formula. Opposite to HNTs, it possesses high density Si—OH on the surface, which makes strong hydrogen bonding interaction exist between OAT nanofibers.[31] Moreover, OAT nanofibers have similar length to HNTs, and the diameter of OAT nanofibers is only

Correspondence to: K.-K. Yang (kkyangscu@126.com).
Contract grant sponsor: National Science Foundation of China; contract grant number: 50873064.
Contract grant sponsor: Program for New Century Excellent Talents in University; contract grant number: NCET-07-0586.
Contract grant sponsor: Funds for Young Scientists of Sichuan Province; contract grant number: 2010JQ0015.

20–30 nm. To estimate the influence of surface character of the clays on the properties of PPDO/clay nanocomposites, PPDO/HNTs nanocomposites were compared with nanocomposites which based on OAT, systematically. Furthermore, the effect of clay content on the properties of the nanocomposites was also discussed, taking PPDO/HNTs nanocomposites as an example.

EXPERIMENTAL

Materials

p-Dioxanone (PDO) was provided by the Pilot Plant of the Center for Degradable and Flame-Retardant Polymeric Materials (Chengdu, People's Republic of China), which was dried over calcium hydride (CaH_2) at room temperature and distilled under reduced pressure until the water content in PDO was under 300 ppm. Triethylaluminum ($AlEt_3$) was purchased from J&K Chemical (Beijing, People's Republic of China). The HNTs was supplied by Beijing Dibaohua Information Technology Co. (Beijing, People's Republic of China) and had been used without any chemical modification. HNTs has typical dimensions 0.5–2 μm in length, 50–70 nm for the outer diameter, and 10–30 nm for the inner diameter. The pristine AT was supplied by Mymine Technology Co. (Anhui, People's Republic of China). AT has typical dimensions 0.5–2 μm in length and 20–30 nm for the diameter. Cetyltrimethylammonium bromide (CTAB) was purchased from Sinopharm Chemical Reagent Co. (Shanghai, People's Republic of China).

Preparation of OAT

CTAB was used as organic modifier for AT. 10.0 g of AT was dispersed in 500 mL distilled water under stirring with ultrasonic agitation to obtain AT suspension at room temperature. Then, 5.0 g CTAB was added into AT suspension with stirring for 24 h at the room temperature. The filtrated product was repeatedly washed with distilled water until no AgBr precipitate occurred when $AgNO_3$ (0.1 mol/L) was added in filtrate. At last, the filtrated cakes were then freeze-dried, and the OAT powders were screened by 200-mesh sieve before use.

Preparation of nanocomposites

Nanocomposites were prepared by the *in-situ* ring-opening polymerization of PDO catalyzed by $AlEt_3$ in the presence of clays. The desired amount of clays was placed in a flame-dried and nitrogen-purged round-bottom flask equipped with a stirrer and a rubber septum. Then the flask was dried by flame and purged by nitrogen three times. The quantitative PDO was added with an injector, and the reaction medium was stirred at 50°C for 3 h and another 1 h with ultrasonic action. Then, the catalyst, a solution of $AlEt_3$ in heptane, was added. The molar ratio of the initial monomer to $AlEt_3$ was 400. The polymerization was conducted at 60°C for 6 h.

TABLE I
Polymerization of PDO in the Presence of Clay ($[Monomer]_0/[AlEt_3]$ = 400, Time = 6 h, Temperature = 60°C)

Samples	Clay content (wt %)	[η] (dL/g)
PPDO	0	2.05
PPDO/1%HNTs	1	1.92
PPDO/3%HNTs	3	1.61
PPDO/5%HNTs	5	1.28
PPDO/7%HNTs	7	1.26
PPDO/10%HNTs	10	1.01
PPDO/3%OAT	3	2.47

Characterization

As the conventional solvents such as chloroform and tetrahydrofuran used in gel permeation chromatography measurements cannot dissolve PPDO with high molecular weights, the intrinsic viscosity [η] of neat PPDO and its nanocomposites was measured in phenol/1,1,2,2-tetrachloroethane (1 : 1 v/v) solution using an Ubbelohde viscometer maintained at 30°C. The test results are presented in Table I.

X-ray diffraction (XRD) analyses were performed on a X'pert diffractometer (Philips, Netherlands), which had an X-ray generator of 3-kW, graphite monochromatic, Cu Kα radiation (wavelength = 1.5406 Å) and was operated at 40 kV and 20 mA. XRD pattern of neat PPDO and its nanocomposites was evaluated from 1-mm thick plates which were prepared by injection molding. The samples were scanned at room temperature from 2° to 40° at a scanning rate of 2°/min.

Scanning electron microscopy (SEM) images were recorded with a FEI Inspect F Scanning Electron Microscope (Philips, Netherlands) operated at 5 kV. All specimens were sputter coated with gold before examination.

The crystallization behavior of PPDO and its nanocomposites was studied by DSC Q200 (TA Instruments, USA). For nonisothermal crystallization, the samples were kept isothermally at 140°C for 5 min to erase previous thermal history, cooled to −50°C at 10°C/min, heated up to 140°C at 10°C/min, then held at 140°C for 3 min again to erase any thermal history, and cooled to −10°C at different constant cooling rates ranging from 1.25 to 10°C/min. The crystallization peak temperature was

obtained from the cooling traces. For isothermal crystallization, the samples were heated to 140°C for 5 min to erase previous thermal history, and then quenched to the isothermal crystallization temperature (T_c), held until the isothermal crystallization completed. The exothermal traces were recorded for the later data analysis.

Polarized optical microscopy (POM) studies were carried out with a ECLIPSE LV100POL microscope (Nikon, Japan) in conjunction with a HSC621V hot stage (Instec, USA). The specimens were heated to 140°C on a hot stage for 3 min, and then quickly cooled to crystallization temperature. The photographs were taken by a digital camera.

Thermogravimetric analysis (TGA) was performed on TG 209 F1 (NETZSCH, Germany) at different constant heating rates ranging from 5 to 25°C/min in a range from ambient temperature to 450°C under a steady flow of nitrogen (50 mL/min).

The rheological measurements were performed on an advanced rheometric expansion system (ARES, TA Instruments, USA) in parallel plate geometry with the diameter of the plates being 25 mm at 130°C. The test samples were pressed into 1-mm thick plates at 140°C. Dynamic oscillatory shear measurements were performed when the angular frequency (ω) range and strain used during testing were 0.05–100 rad s^{-1} and 5%, respectively.

The dynamic mechanical analyses (DMA) were conducted on a DMA Q800 (TA Instruments, USA) in the tension mode using samples of 35 × 4 × 2 mm^3 in size which were prepared by injection molding. The samples were conducted at a cyclic tensile strain with an amplitude of 0.2% at a frequency of 1 Hz and a static force of 0.1 N was used. The temperature was ranged from −50°C to 90°C with a heating rate of 3°C/min.

The dried neat PPDO and its nanocomposites pellets were injection-molded using HAAKE MinJet (Thermo Electron Corporation, USA) operated at 160°C with a mold temperature of 30°C. The mechanical performance was measured by SANS CMT4104 (SANS Group, People's Republic of China) at a crosshead speed of 25 mm/min with GB/T 1040.2-2006 method at room temperature. At least five specimens were tested in each group and the reported values of each group reflected an average of five specimens.

RESULTS AND DISCUSSION

Nanocomposites structure

Figure 1 shows the SEM photographs of the fractured section of nanocomposites. It can be seen that both HNTs and OAT nanofibers distributed uniformly in the fractured section of nanocomposites samples at low content. Aggregation only occurs when HNTs content reach 5%, and HNTs bundles could be observed especially when the content of HNTs is up to 10 wt %. Comparing with HNTs, the dispersion of OAT nanofibers is poorer in PPDO matrix (Figure 2). This phenomenon is due to the unique surface character of OAT nanofibers. Opposite to HNTs, there is high density Si—OH on the surface of OAT nanofibers, which make hydrogen bonding interaction strong among OAT nanofibers. In addition, the edges of HNTs and OAT nanofibers appear to be better dispersed into the surrounding matrix. Moreover, most of HNTs and OAT nanofibers were fractured and only a few HNTs and OAT nanofibers were pulled out from the PPDO matrix. These phenomena indicate both HNTs and OAT nanofibers have good interfacial compatibility with PPDO matrix, which is attributed to the surface character of the clays. In the case of HNTs, the outer surface of HNTs is composed of siloxane, which has similar chemical nature to PPDO molecular chains as repeated ester–ether structure. So there is a well interfacial adhesion between HNTs and PPDO matrix. Concerning OAT, hydroxyl groups on the OAT surface, on the one hand, form hydrogen bonds with PPDO molecular chains, on the other hand, act as polymerization initiators for the ring-opening polymerization of PDO, leading to PPDO chains grafting onto the OAT surface.[3,22–25] And the existence of PPDO chains grafted on the surface of OAT causes entanglement and co-crystallization with the ungrafted PPDO chains. Hence there are strong interactions between OAT and PPDO matrix.

Crystallization behaviors

Spherulitic morphology and structure

The spherulitic morphology of PPDO and its nanocomposites was observed by POM. Figure 3 presents spherulitic morphology of all samples crystallized after full solidification at 70°C. The birefringent ring-banded spherulitic structure can be observed for neat PPDO and its nanocomposites. The gradual decrease of spherulitic size with increasing HNTs loading is clearly observed. This observation suggests that HNTs can serve as a heterogeneous nucleation agent for PPDO crystallization. Nevertheless, it should be noted that the average spherulite size of PPDO/10%HNTs is larger than 50 μm, indicating the nucleation effect of HNTs on PPDO crystallization is limited. From Figure 3, it also can be seen that the nucleation density of PPDO/3%OAT is obviously less than that of PPDO/3%HNTs. This phenomenon may be due to the unique surface character of OAT nanofibers, which possess high density Si—OH on the surface. Hydrogen bonds can be

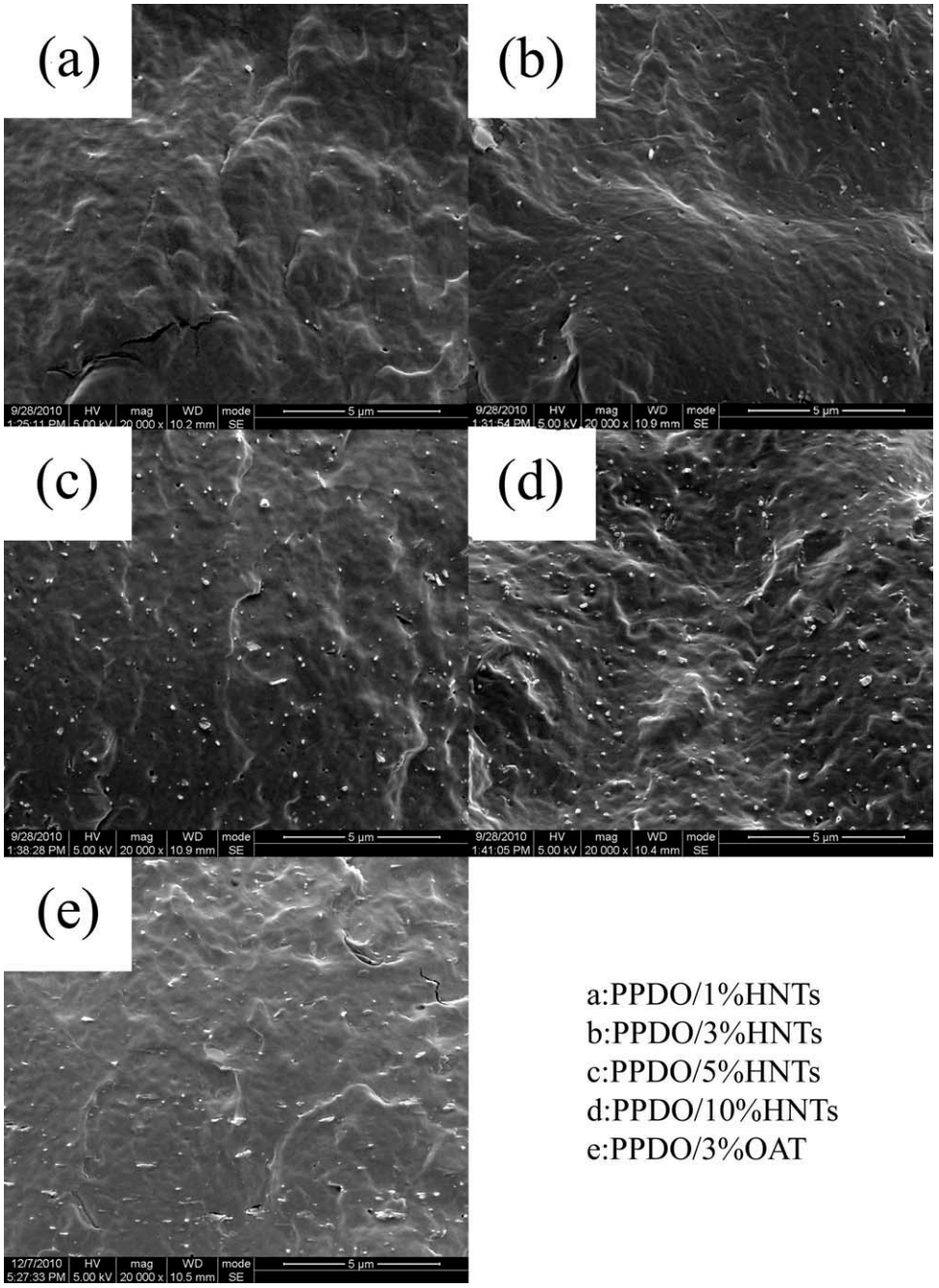

Figure 1 SEM photographs of brittle fracture section of nanocomposites.

formed between Si—OH and PPDO molecular chains. So, the motion of the PPDO molecular chains around OAT nanofibers was restricted, and it needed to overcome an energy barrier to drive the nucleating and growing, resulting that the heterogeneous nucleation capability of OAT was limited. Despite of more agglomerates in PPDO/OAT nanocomposites, the nucleation effect of OAT on PPDO crystallization is weaker than that of HNTs in its nanocomposites.

The effect of clay incorporation on the crystal structure of PPDO in the nanocomposites was studied by XRD. Figure 4 illustrates the XRD patterns of neat PPDO and its nanocomposites, which were crystallized at 70°C for 24 h. As shown in Figure 4, all nanocomposites samples show three main characteristic diffraction peaks at $2\theta = 21.9°$, 23.7°, 29.3° as neat PPDO does,[32] which are attributed to the reflection of (210), (020), and (310), respectively. In addition, it also should be noticed that the intensities of the diffraction peaks of PPDO were reinforced when the loading of HNTs and OAT was below 5 wt %, and reduced gradually when HNTs content reach or beyond 5 wt %. To illustrate this phenomenon

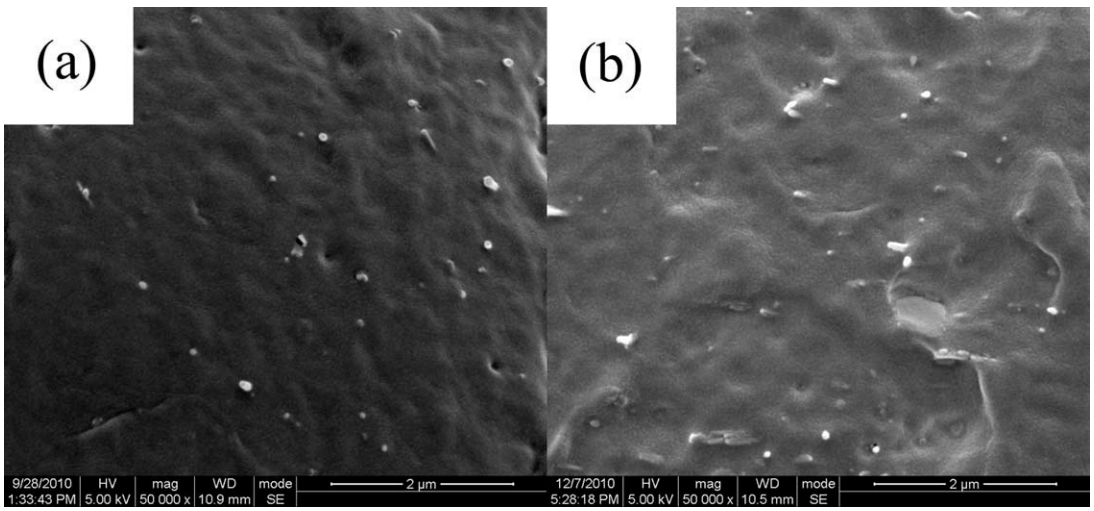

Figure 2 High magnification SEM photographs of (a) PPDO/3%HNTs and (b) PPDO/3%OAT.

quantitatively, the ratios of diffraction peak intensity of PPDO matrix in nanocomposites to that of neat PPDO (I_r) are summarized in Table II. Apparently, the incorporation of low clay contents led to an increase in crystallinity and a gradual decrease in degree of crystallinity and crystalline order occurred at high clay content. These results suggest the addition of clay does not modify the crystal structure of PPDO but reduces the ultimate extent of bulk crystallinity of PPDO at high clay content.

Nonisothermal crystallization behavior

Figure 5 illustrates the DSC traces for neat PPDO and its nanocomposites, and all the relevant data are summarized in Table III. As shown in Figure 5(a), the melt crystallization peaks gradually strengthen and the melt crystallization temperature (T_{c1}) tends to shift to high temperature with increasing HNTs content. And when HNTs content reach or beyond 5 wt %, no cold crystallization peaks can be observed in Figure 5(b). These results show that the incorporation of HNTs enhances the nonisothermal crystallization of the PPDO matrix. Comparing with PPDO/3%HNTs, melt crystallization peak of PPDO/3%OAT is obviously smaller, suggesting the enhancement effect of OAT on nonisothermal melt crystallization of PPDO is worse than that of HNTs. This result is attributed to the heterogeneous nucleation capability of OAT restricted by hydrogen bonds. In addition, it can be seen from the Table IV that the absolute degree of crystallinity of PPDO/HNTs nanocomposites is higher than that of neat PPDO and gradually decreases with increasing HNTs content, due to restricted motion of PPDO molecular chains by HNTs. As a result of strong hydrogen bonding interaction between OAT nanofibers and PPDO molecular chains, the absolute degree of crystallinity of PPDO/3%OAT is lower than that of neat PPDO.

To investigate the effect of cooling rate on the nonisothermal melt crystallization, Figure 6 summarizes the variation of crystallization peak temperature (T_p) with cooling rate (Φ) for neat PPDO and its nanocomposites. It is obvious that T_p shifts to low temperature with increasing cooling rate for both neat PPDO and its nanocomposites; moreover, T_p shifts to high temperature with increasing the HNTs contents in the nanocomposites. In the case of PPDO/3%OAT, it should be noticed that T_p of PPDO/3%OAT is clearly lower than that of neat PPDO at high cooling rate. Since PPDO molecular chains are difficult to move and arrange at high cooling rate and the existence of OAT hinders the movement of PPDO molecular chains, PPDO molecular chains are difficult to fold on the surface of OAT to form nucleus and arrange into lamellae. In addition, T_p of PPDO/3%OAT is lower than that of PPDO/3%HNTs at a given cooling rate, due to the heterogeneous nucleation capability of OAT restricted by hydrogen bonds. From the above mentioned studies, it is clear that the presence of HNTs and their contents have a significant effect on the nonisothermal melt crystallization behavior of PPDO in nanocomposites due to the heterogeneous nucleation agent effect of HNTs.

Isothermal crystallization behavior

The isothermal crystallization of neat PPDO and its nanocomposites at 70°C was also investigated by DSC. Figure 7(a) shows the plots of relative crystallinity versus crystallization time for neat PPDO and its nanocomposites. The Avrami equation is used to analyze the isothermal crystallization kinetics of neat PPDO and its nanocomposites. It assumes that the

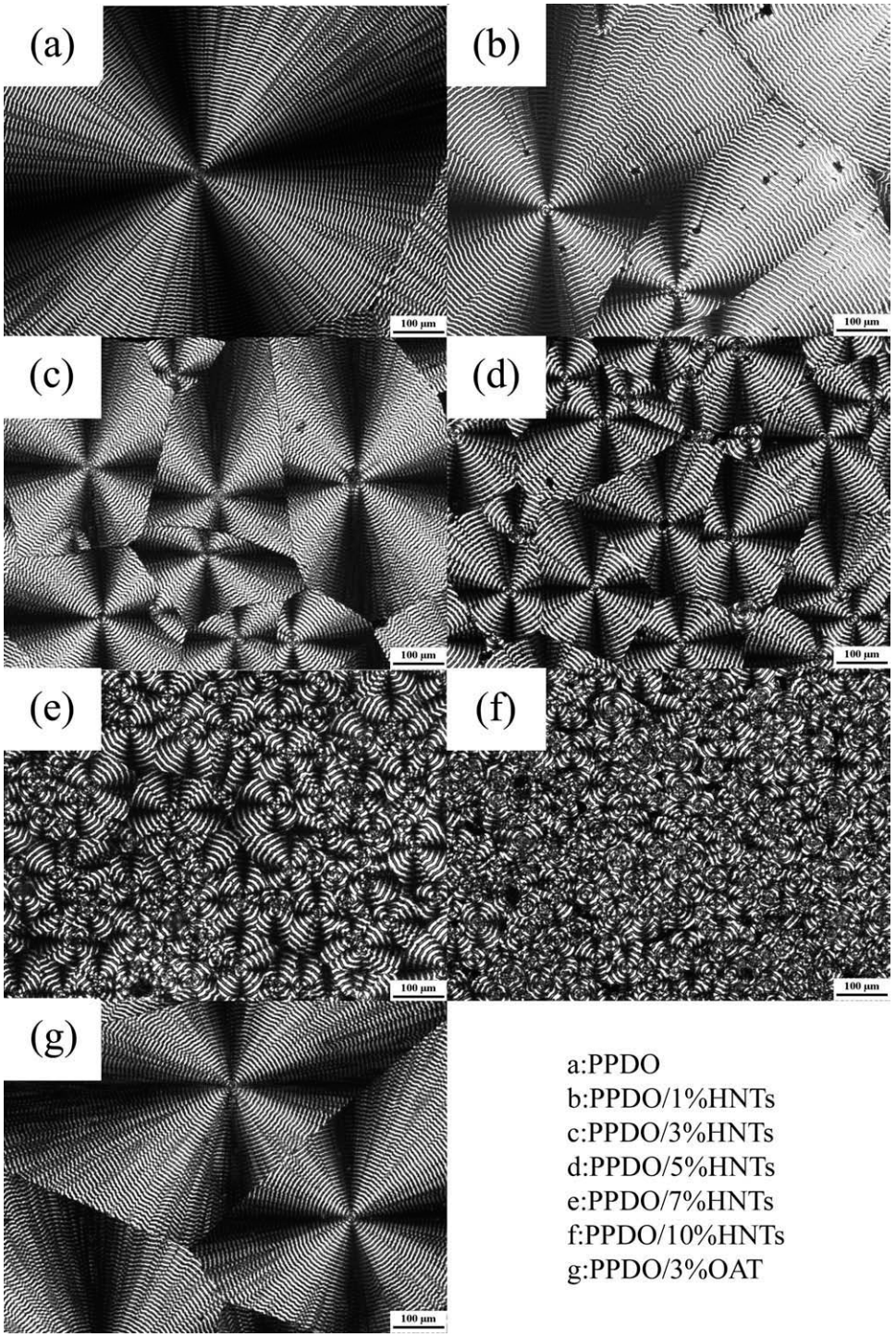

Figure 3 Optical micrographs of neat PPDO and its nanocomposites crystallized after full solidification at 70°C.

relative degree of crystallinity X_t develops as a function of crystallization time t as follows:[34]

$$1 - X_t = \exp(-kt^n) \tag{1}$$

where X_t is the relative degree of crystallization, n is the Avrami exponent, and k is a composite rate constant involving both nucleation and growth rate parameters, These parameters are related to the crystallization half-time $t_{0.5}$. The value of $t_{0.5}$ is calculated by the following equation:

$$t_{0.5} = \left(\frac{\ln 2}{k}\right)^{1/n} \tag{2}$$

All the isothermal crystallization kinetics parameters of PPDO and its nanocomposites are summarized in Table IV. From Table IV, it can be seen that

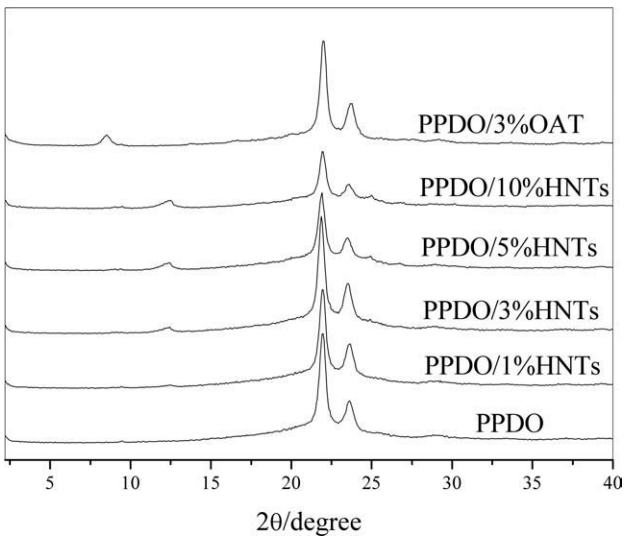

Figure 4 XRD patterns of neat PPDO and its nanocomposites.

the values of n are closed to 3 for the isothermal crystallization of both neat PPDO and its nanocomposites, suggesting spherulitic growth. Moreover, the nonintegral n value between 2 and 4 may reflect the crystal branching and/or mixed crystal growth and nucleation mechanism.[35] And the average values of n increase with the increasing content of HNTs, revealing the incorporation of HNTs causes heterogeneous athermal nucleation followed by higher crystal branching in spherulitic growth. On the other hand, the values of k increase with increasing HNTs loading, indicating that the incorporation of HNTs enhances the crystallization rate of PPDO. The increase of crystallization rate of PPDO in its nanocomposites is attributed to the increased nucleation rate of PPDO in nanocomposites.

Usually, the crystallization rate can also be easily described by the reciprocal of $t_{0.5}$. As shown in Table IV, the values of $t_{0.5}$ decrease monotonically with the increase of HNTs content; corresponding, the values of $1/t_{0.5}$ increase, indicating again that the addition of HNTs accelerates the crystallization process of PPDO and HNTs has a significant effect on accelerating the crystallization of PPDO. Owing to the heterogeneous nucleation capability of OAT restricted in nanocomposites, $t_{0.5}$ of PPDO/3%OAT is obviously longer than that of PPDO/3%HNTs.

TABLE II
XRD Peak Intensity of Neat PPDO and Its Nanocomposite, and the Ratio of Diffraction Peak Intensity of PPDO Matrix in Nanocomposites to That of Neat PPDO

Samples	I_{020}	I_r[a]
PPDO	2788	1.000
PPDO/1%HNTs	2972	1.077
PPDO/3%HNTs	3324	1.299
PPDO/5%HNTs	2233	0.843
PPDO/10%HNTs	1678	0.669
PPDO/3%OAT	2879	1.065

[a] The ratio of diffraction peak intensity of PPDO matrix in nanocomposites to that of neat PPDO, $I_r = I_{020}/(1 - \phi) I_0$. I_0 is the diffraction peak intensity of neat PPDO. ϕ is the weight fraction of clay.

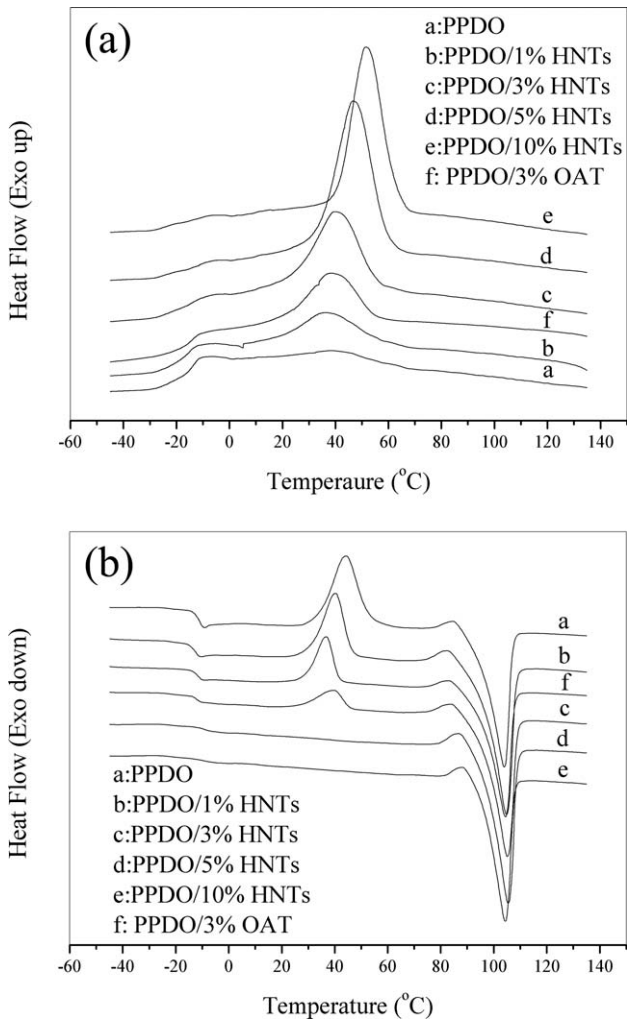

Figure 5 DSC scans of neat PPDO and its nanocomposites: (a) cooling scans and (b) heating scans.

Thermal stability

The thermal stability of neat PPDO and its nanocomposites in nitrogen was studied by TG. Figure 8 shows TGA and DTG curves of neat PPDO and its nanocomposites at heating rate 10°C/min, and the characteristic weight loss temperatures are summarized in Table V. To investigate the influence of the clays on the thermal stability of PPDO, the temperature at 5% weight loss ($T_{5\%}$) and the temperature at 50% weight loss ($T_{50\%}$) for all samples were recorded for comparison. From Table V, it can be seen that $T_{50\%}$ of PPDO/HNTs nanocomposites increases with

TABLE III
DSC Date for Neat PPDO and Its Nanocomposites

Samples	T_{c1} (°C)	ΔH_{c1} (J/g)	T_{c2} (°C)	ΔH_{c2} (J/g)	T_g (°C)	T_m (°C)	ΔH_m (J/g)	χ_c[a] (%)
PPDO	39.5	8.6	44.3	44.2	−11.0	104.0	53.2	37.7
PPDO/1%HNTs	36.7	20.0	40.1	33.7	−11.4	104.8	60.2	43.1
PPDO/3%HNTs	39.9	41.3	39.9	12.0	−11.9	105.0	57.8	42.2
PPDO/5%HNTs	46.6	62.0	/	/	−9.3	105.4	55.7	41.5
PPDO/10%HNTs	51.5	57.2	/	/	−9.9	104.2	50.7	39.9
PPDO/3%OAT	38.3	26.5	36.7	20.2	−11.6	104.5	50.8	37.1

[a] The absolute degree of crystallinity, χ_c (%) = 100 × $\Delta H_m/(1 - \phi)\ \Delta H_m^0$. ϕ is the weight fraction of clay, and ΔH_m^0 is the melting enthalpy of 100% crystalline PPDO (141.2 J g^{-1}).[33]

increasing HNTs loading. Furthermore, a gradual decrease in mass loss rate can be observed in Figure 8(b), indicating that the presence of HNTs hinders the formation of small molecules and their escape from nanocomposites. These results show that the addition of HNTs enhances the thermal stability of PPDO and HNTs has a significantly effect on enhancing the thermal stability of PPDO. However, above 5 wt % HNTs, $T_{5\%}$ of PPDO/HNTs nanocomposites shifts to lower temperatures with an increase in the HNTs content continuously. Chemical analysis shows the presence of Fe^{3+} in the HNTs,[36] which acted as an inhibitor for the polymerization of PDO. So the molecular weight distribution of PPDO in nanocomposites gradually become wider with increasing HNTs contents, due to the increased concentration of Fe^{3+} in the reaction system. At high HNTs content (>5 wt % HNTs), the amount of low molecular weight PPDO in nanocomposites is enough to reduce the thermal stability. It should be noticed in Table V that $T_{5\%}$ and $T_{50\%}$ of PPDO/3%OAT is lower than that of PPDO/3%HNTs, especially $T_{5\%}$. This result is attributed to the unique surface character of OAT nanofibers, which possess high density Si—OH on the surface. It is well known that the decomposition of PPDO proceeds by unzipping depolymerization as main reaction.[37] However, in the initial stages, the decomposition of PPDO is mainly leaded by the random reactions because its repeated aliphatic ester–ether structure is relatively easy to hydrolyze.[38] The Si—OH on the OAT surface accelerates decomposition of ester group in PPDO.

To study the effect of HNTs in thermal decomposition process of PPDO nanocomposites, the TGA and DTG curves were obtained at different heating rate. As shown in Figure 9(b′), another decomposition peak is gradually apparent in the DTG curve of PPDO/10%HNTs with increasing heating rate, suggesting that the thermal decomposition process of PPDO/HNTs nanocomposites is divided into two stages. This phenomenon is due to the hollow tubular structure of HNTs. As reported,[39] the volume percentage of the cavity of HNTs is up to 25%, and HNTs is an effective barrier for heat transport. A considerable part of PPDO molecules synthesized directly in the lumen of HNTs via the *in-situ* ring-opening polymerization of PDO, resulting effective delay in mass transport and remarkably increased thermal stability. The thermal decomposition process of PPDO/HNTs nanocomposites can be divided into following two stages: (a) the diffusion of decomposition products of PPDO molecular chains which were not restricted by HNTs in PPDO matrix; (b) the

TABLE IV
Crystallization Kinetic Parameters for Neat PPDO and Its Nanocomposites at 70°C

Samples	n	k (min^{-n})	$t_{0.5}$ (min)	$1/t_{0.5}$ (min^{-1})
PPDO	2.90	7.638×10^{-5}	23.09	0.04331
PPDO/1%HNTs	3.14	3.126×10^{-4}	11.61	0.08613
PPDO/3%HNTs	3.34	4.955×10^{-4}	8.752	0.1143
PPDO/5%HNTs	3.49	1.871×10^{-3}	5.444	0.1837
PPDO/10%HNTs	3.35	5.821×10^{-3}	4.167	0.2400
PPDO/3%OAT	3.20	5.047×10^{-4}	10.72	0.09328

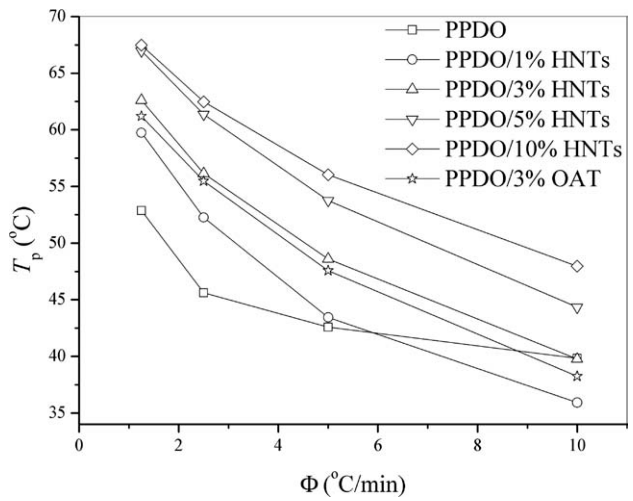

Figure 6 Effect of cooling rates on the crystallization peak temperatures for neat PPDO and its nanocomposites.

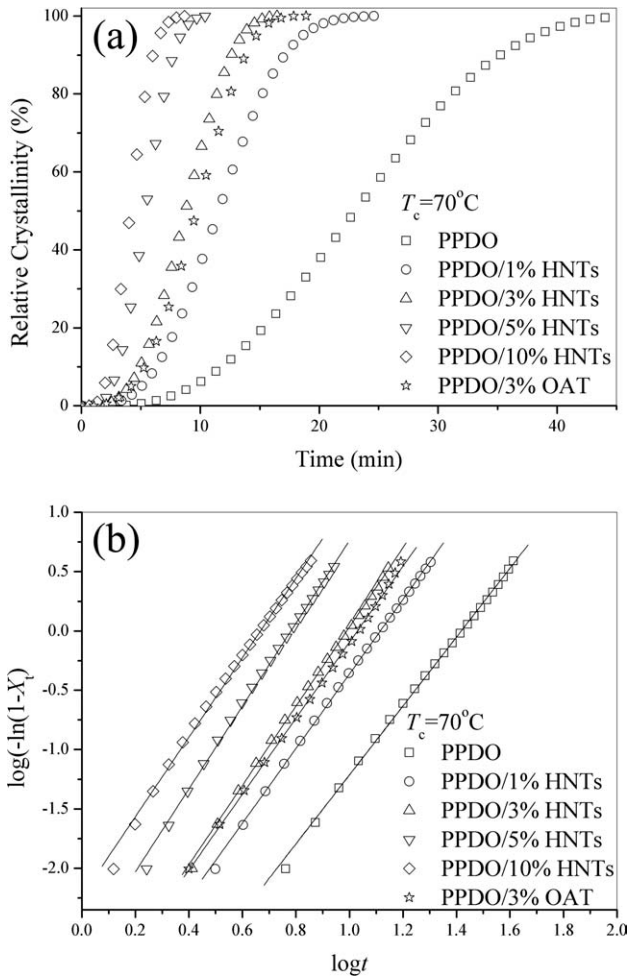

Figure 7 Effect of clay on the crystallization of PPDO at 70°C: (a) development of relative crystallinity with crystallization time; (b) the Avrami plots.

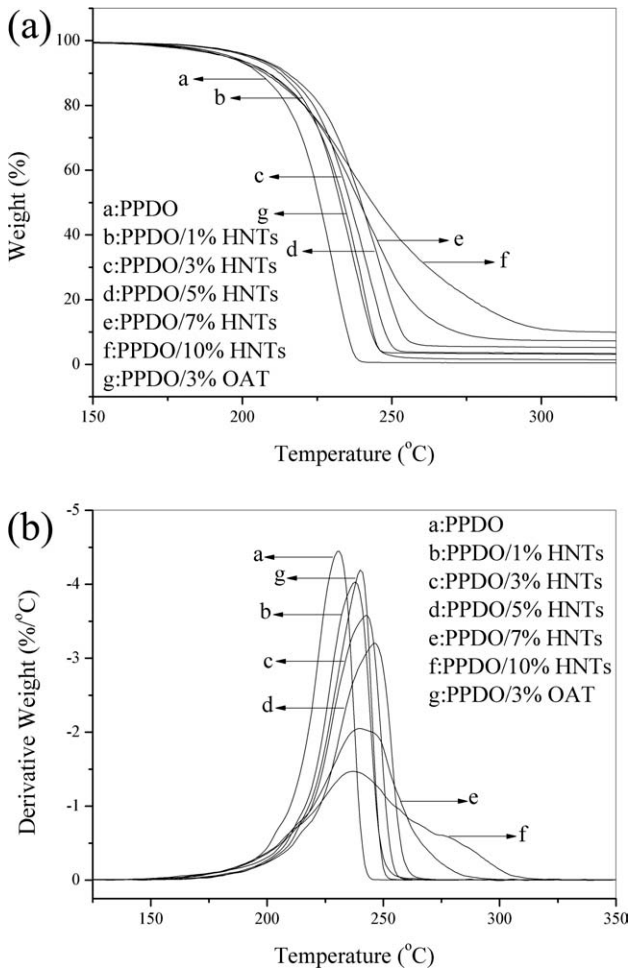

Figure 8 TGA and DTG curves of neat PPDO and its nanocomposites: (a) TGA curves and (b) DTG curves.

diffusion of decomposition products of PPDO molecular chains restricted by HNTs.

Rheological properties

The measurement of rheological properties of polymeric materials at molten state is crucial to gain fundamental understanding of the processability and the structure–property relationship for these materials. The linear dynamic viscoelastic master curves for neat PPDO and its nanocomposites are shown in Figure 10. As shown in Figure 10(b), a significant drop of complex viscosities ($|\eta^*|$) occurs when the content of HNTs is up to 5 wt %, and further increase in HNTs results in a continuous decrease $|\eta^*|$ of nanocomposites. This behavior is contrasted with that of the PPDO/MMT nanocomposites, in which it was noted that $|\eta^*|$ of nanocomposites was higher than neat PPDO. It is well known that the rheological properties of polymer/clay nanocomposites is sensitive to interactions between the clay surfactant and the polymer.[40] This different rheological behaviors may be ascribed to the unique outer surface structure of HNTs, which is mainly composed of O—Si—O groups. Compared with other silicates such as MMT, the density of outer surface hydroxyl groups of HNTs is much smaller. Therefore, the interaction between HNTs and PPDO matrix is relatively weak. It is reasonable to believe that HNTs acted as a barrier to disrupt the entanglements of PPDO molecular chains by physically separating them in PPDO melt, thus resulting in lower

TABLE V
The TGA Data for Neat PPDO and Its Nanocomposite

Samples	$T_{5\%}$ (°C)	$T_{50\%}$ (°C)	$T_{75\%}$ (°C)
PPDO	195.1	225.9	231.5
PPDO/1%HNTs	202.3	232.7	239.0
PPDO/3%HNTs	203.5	236.0	243.2
PPDO/5%HNTs	204.0	239.8	247.8
PPDO/7%HNTs	196.6	239.3	252.3
PPDO/10%HNTs	195.0	243.4	268.8
PPDO/3%OAT	195.1	233.9	240.2

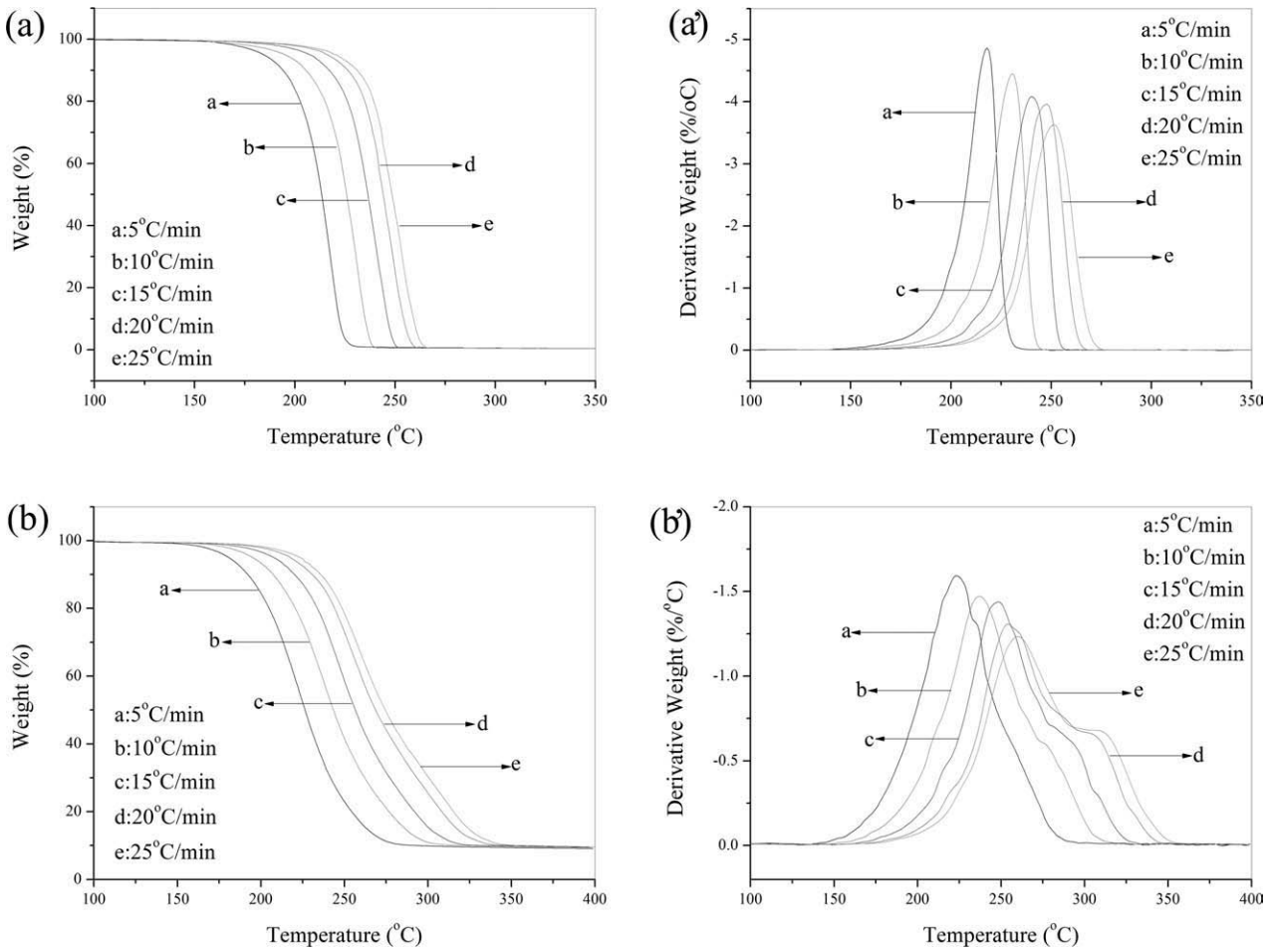

Figure 9 TGA and DTG curves of neat PPDO and its nanocomposites at different heating rate: (a) TGA curves of neat PPDO, (b) TGA curves of PPDO/10%HNTs, (a') DTG curves of neat PPDO, and (b') DTG curves of PPDO/10%HNTs.

complex viscosity. Opposite to HNTs, the addition of OAT makes $|\eta^*|$ improved significantly, due to the high density of hydroxyl groups on the surface of OAT. A part of PPDO molecules is grown directly from Si—OH groups of OAT by surface-initiated, ring-opening polymerization of PDO. Hence, there are strong interactions between the OAT surface and PPDO matrix, leading to higher $|\eta^*|$. Moreover, the storage modulus (G') is also enhanced by addition of OAT. This character somewhat would improve the processability of materials. In addition, it also should be noticed in Figure 10(a) that the decreasing trend for G' is similar to that for $|\eta^*|$ in PPDO/HNTs nanocomposites, and the addition of clay does not change the shape and slope of the G' curves, indicating unaltered chain dynamics greatly.

Thermomechanical properties and tensile properties

Thermomechanical properties of neat PPDO and its nanocomposites have been investigated by DMA as a function of clay content and temperature. Figure 11(a) shows the temperature dependence of the storage modulus for neat PPDO and its nanocomposites. For all nanocomposites samples, a significant enhancement of storage modulus can be seen in the investigated temperature range, indicating incorporation of clay has a strong effect on the elastic properties of the PPDO matrix. In the case of PPDO/HNTs nanocomposites, storage modulus of nanocomposites gradually increases with increasing HNTs content at high temperature. For instance, the increases in storage modulus are 41.9% for PPDO/3%HNTs, 59.6% for PPDO/7%HNTs, and 74.2% for PPDO/10%HNTs as compared with that of neat PPDO at 30°C. This increase may be attributed to the high intrinsic stiffness of HNTs, resulting from their tube-like geometry. Obviously, the stiffness of nanocomposites is mainly affected by two factors as follows: the intrinsic stiffness of nanoparticles, and interfacial interaction between surface of nanoparticles and polymer matrix.[41] However, there are only weak interfacial interactions between the surface of

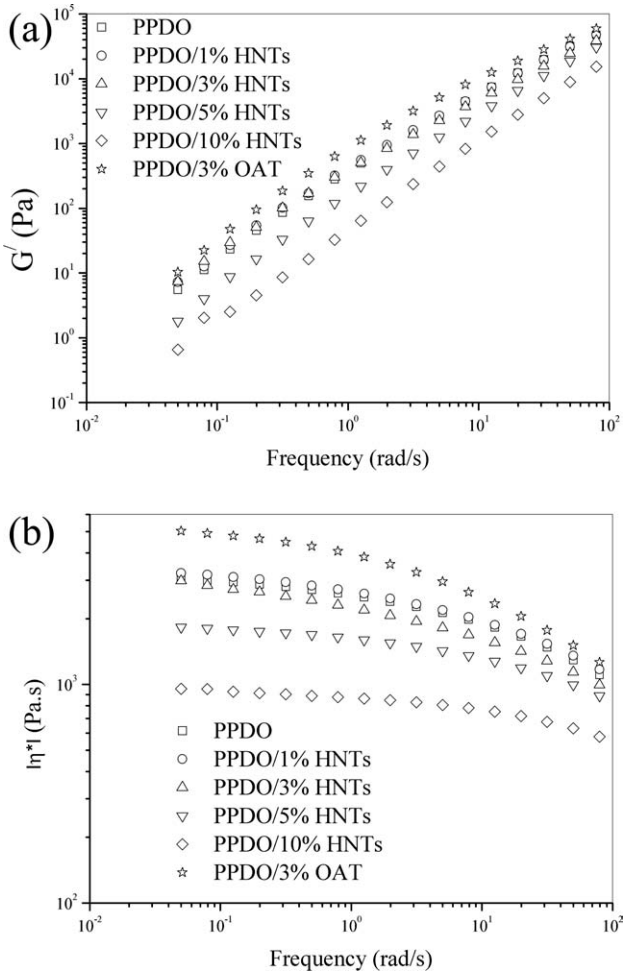

Figure 10 Frequency dependence of storage modulus [G′], and complex viscosity [|η*|] of neat PPDO and its nanocomposites at 130°C.

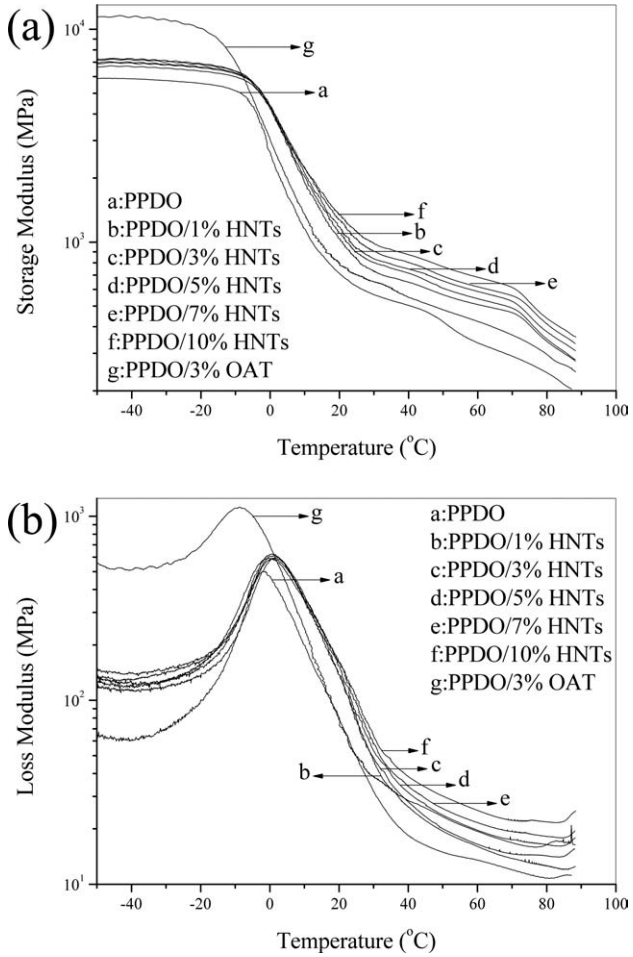

Figure 11 DMA curves of neat PPDO and its nanocomposites: (a) storage modulus as a function of temperature; (b) loss modulus as a function of temperature.

HNTs and PPDO matrix, due to the inert outer surface of HNTs. Moreover it should be noticed the storage modulus shows a greater enhancement at high temperature than at low temperature. At high temperature ($>T_g$), the motion ability of PPDO molecular chains is gradually improved with increasing temperature, resulting in PPDO matrix becoming softer. Meanwhile, the effect of the intrinsic stiffness of HNTs on stiffness of nanocomposites becomes prominent. Different from PPDO/HNTs nanocomposites, PPDO/OAT nanocomposites show a greater increase in storage modulus at low temperature, due to the strong interfacial interaction between OAT and PPDO matrix. At low temperature ($<T_g$), the reinforcement effect of the clay particles is mainly determined by the interfacial interaction between the surface of clay particles and polymer matrix when polymer chains are frozen. The improvement of interfacial interaction leads to increase in cohesive

TABLE VI
The Tensile Properties of Neat PPDO and Its Nanocomposites

Samples	Stress at yield (MPa)	Stress at break (MPa)	Strain at break (%)	Young's modulus (MPa)
PPDO	28.4 ± 0.5	46.3 ± 2.2	289 ± 13	353 ± 17
PPDO/1%HNTs	29.1 ± 0.6	56.6 ± 0.5	343 ± 10	434 ± 23
PPDO/3%HNTs	28.8 ± 0.4	59.9 ± 1.3	420 ± 12	503 ± 23
PPDO/5%HNTs	29.5 ± 0.8	55.1 ± 1.4	443 ± 7	558 ± 30
PPDO/7%HNTs	29.8 ± 0.7	51.9 ± 1.1	406 ± 18	652 ± 28
PPDO/10%HNTs	29.4 ± 0.3	46.2 ± 1.7	358 ± 11	711 ± 13
PPDO/3%OAT	34.7 ± 1.4	59.6 ± 1.0	398 ± 14	509 ± 8

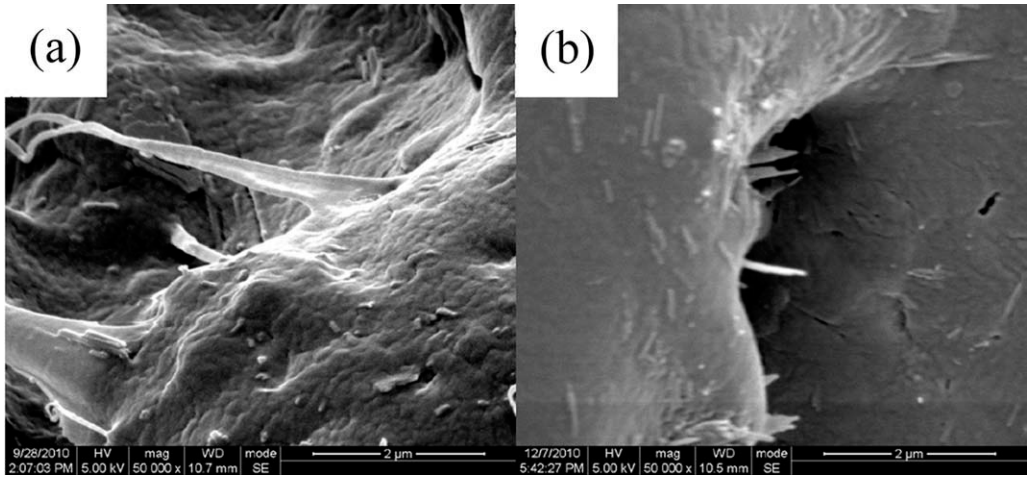

Figure 12 SEM pictures taken on the fracture surfaces from tensile testing of the nanocomposites with 3 wt % clay showing: (a) PPDO/3%HNTs and (b) PPDO/3%OAT.

energy density of polymer in nanocomposites, resulting in higher modulus.[42] In addition, Figure 11(b) illustrates loss modulus as a function of temperature for neat PPDO and its nanocomposites. Loss modulus is a measure of the energy absorbed due to a relaxation, and the value of the glass transition temperature (T_g) can be determined by the peak temperature of loss modulus. The values of T_g is −1.78°C for neat PPDO, 0.57°C for PPDO/3%HNTs, and −8.64 for PPDO/3%OAT, respectively. Evidently, T_g is improved by the addition of HNTs and reduced by the addition of OAT. Generally, the incorporation of clay into the polymer matrix is found to improve T_g by restricting mobility of polymer chain segments. However, the opposite effect is found in the case of PPDO/OAT nanocomposites. This decrease in T_g is probably due to the plasticizing effect from the organic modifier and low molecular weight OAT-grafted PPDO within OAT, and similar results have been reported in the literature.[43,44]

Tensile tests were also performed to characterize the tensile properties of neat PPDO and its nanocomposites, and test results are summarized in Table VI. As shown in Table VI, tensile strength, elongation at break and Young's modulus of nanocomposites is obviously higher than that of neat PPDO, indicating nanocomposites are reinforced and toughened by the addition of clay. Comparing with OAT, HNTs has a better toughening effect on PPDO matrix. The elongation at break of PPDO/HNTs nanocomposites is improved by 45.3% when 3 wt % HNTs is added, while only limited improvement (37.7%) is observed at the same weight fraction of OAT loading. Even when the content of HNTs is up to 10 wt %, the elongation at break of its nanocomposites is still up 23.9% over that of neat PPDO. This phenomenon can be ascribed to well dispersion of HNTs in low content. Furthermore, from the Figure 12, it is can be seen that both HNTs and OAT nanofibers act as crack-bridging in nanocomposites, resulting from interactions between clay and PPDO matrix.[45] The failure mechanisms of crack-bridging are responsible for the improved ductility of nanocomposites with the clays. However, it is worth mentioning that both tensile strength and elongation at break gradually decrease with an increase in HNTs loading when HNTs content reach or beyond 5 wt %, due to the stronger tendency of HNTs to agglomerate at higher HNTs content. The formation of HNTs agglomerates in nanocomposites results in a reduction of the effective surface area which can undergo matrix–filler interactions, moreover, HNTs agglomerates in the nanocomposites can act as the stress concentration sites where the cracks will generate.

CONCLUSIONS

The nanocomposites of PPDO with HNTs or OAT, which have different surface character, were prepared by *in-situ* ring-opening polymerization. Both HNTs and OAT nanofibers dispersed uniformly in PPDO matrix. By comparing the two tested clays, it was found that HNTs was more effective in improving the crystallization rate, thermal stability as well as the mechanical performance, and OAT was more effective in improving the rheological behavior. In addition, the crystallization rate, and rigidity of nanocomposites increased with increasing HNTs loading.

References

1. Yang, K. K.; Wang, X. L.; Wang, Y. Z. J Macromol Sci Polym Rev 2002, 42, 373.
2. Huang, H. X.; Yang, K. K.; Wang, Y. Z.; Wang, X. L.; Jun, L. J Polym Sci Part A: Polym Chem 2006, 44, 1245.

3. Yoon, K. R.; Lee, K. B.; Chi, Y. S.; Yun, W. S.; Joo, S. W.; Choi, I. S. Adv Mater 2003, 15, 2063.
4. Sabino, M. A.; Albuerne, J.; Muller, A. J.; Brisson, J.; Prudhomme, R. E. Biomacromolecules 2004, 5, 358.
5. Yang, K. K.; Wang, X. L.; Wang, Y. Z.; Huang, H. X. Mater Chem Phys 2004, 87, 218.
6. Bhattarai, S. R.; Yi, H. K.; Bhattarai, N.; Hwang, P. H.; Kim, H. Y. Acta Biomater 2006, 2, 207.
7. Bhattarai, S. R.; Bhattarai, N.; Yi, H. K.; Hwang, P. H.; Cha, D. I.; Kim, H. Y. Biomaterials 2004, 25, 2595.
8. Yomeda, M.; Terai, H.; Imai, Y.; Okada, T.; Nozaki, K.; Inoue, H.; Miyamoto, S.; Takaoka, K. Biomaterials 2005, 26, 5145.
9. Raquez, J. M.; Degee, P.; Dubois, P.; Balakrishnan, S.; Narayan, R. Polym Eng Sci 2005, 45, 622.
10. Bhattarai, N.; Jiang, W. Y.; Kim, H. Y.; Lee, D. R.; Park, S. J. J Polym Sci Part B: Polym Phys 2004, 42, 2558.
11. Mohammadi-Rovshandeh, J. Scienceasia 2008, 34, 207.
12. Li, Y. D.; Chen, S. C.; Zeng, J. B.; Wang, Y. Z. Ind Eng Chem Res 2008, 47, 8233.
13. Zhou, Y. F.; Yang, K. K.; Wang, Y. Z.; Wang, X. L. Polym Bull 2006, 57, 151.
14. Zheng, L.; Wang, Y. Z.; Yang, K. K.; Wang, X. L.; Chen, S. C.; Li, J. Eur Polym J 2005, 41, 1243.
15. Wang, X. L.; Yang, K. K.; Wang, Y. Z.; Wang, D. Y.; Yang, Z. Acta Mater 2004, 52, 4899.
16. Huang, F. Y.; Wang, Y. Z.; Wang, X. L.; Yang, K. K.; Zhou, Q.; Ding, S. D. J Polym Sci Part A: Polym Chem 2005, 43, 2298.
17. Yang, K. K.; Zhou, Y.; Lu, F.; Huang, F. Y.; Qiu, Z. C.; Wang, Y. Z. J Macromol Sci Part B: Phys 2009, 48, 1031.
18. Qiu, Z. C.; Zhang, J. J.; Zhou, Y.; Song, B. Y.; Chang, J. J.; Yang, K. K.; Wang, Y. Z. Polym Adv Technol 2011, 22, 993.
19. Zubitur, M.; Fernández, A.; Mugica, A.; Cortázar, M. Phys Status Solidi A 2008, 205, 1515.
20. Zubitur, M.; Gomez, M. A.; Cortazar, M. Polym Degrad Stab 2009, 94, 804.
21. Zubitur, M.; Mugica, A.; Areizaga, J.; Cortazar, M. Colloid Polym Sci 2010, 288, 809.
22. Yoon, K. R.; Kim, W. J.; Choi, I. S. Macromol Chem Phys 2004, 205, 1218.
23. Yoon, K. R.; Koh, Y. J.; Choi, I. S. Macromol Rapid Commun 2003, 24, 207.
24. Yoon, K. R.; Chi, Y. S.; Lee, K. B.; Lee, J. K.; Kim, D. J.; Koh, Y. J.; Joo, S. W.; Yun, W. S.; Chio, I. S. J Mater Chem 2003, 13, 2910.
25. Yoon, K. R.; Kim, Y.; Choi, I. S. J Polym Res 2004, 11, 265.
26. Alexandre, M.; Dubois, P. Mater Sci Eng R 2000, 28, 1.
27. Sahoo, N. G.; Rana, S.; Cho, J. W.; Li, L.; Chan, S. H. Prog Polym Sci 2010, 35, 837.
28. Spitalsky, Z.; Tasis, D.; Papagelis, K.; Galiotis, C. Prog Polym Sci 2010, 35, 357.
29. Joussein, E.; Petit, S.; Churchman, J.; Theng, B.; Righi, D.; Delvaux, B. Clay Miner 2005, 40, 383.
30. Frost, R. L.; Shurvell, H. F. Clays Clay Miner 1997, 45, 68.
31. Murray, H. H. Appl Clay Sci 2000, 17, 207.
32. Furuhashi, Y.; Nakayama, A.; Monno, T.; Kawahara, Y.; Yamane, H.; Kimura, Y.; Iwata, T. Macmol Rapid Commun 2004, 25, 1943.
33. Ishikiriyama, K.; Pyda, M.; Zhang, G. E.; Forschner, T.; Grebowicz, J.; Wunderlich, B. J. Macromol Sci Part B Phys 1998, 37, 27.
34. Avrami, M. J Chem Phys 1939, 7, 1103.
35. Wunderlich, B. Macromolecular Physics; Academic Press: New York, 1976; Vol. 2.
36. Technical Report of Imerys Tableware Asia Limited. Available at: http://www.imerys-tableware.com/halloy.html. Accessed on November 7, 2009.
37. Nishida, H.; Yamashita, M.; Hattori, N.; Endo, T.; Tokiwa, Y. Polym Degrad Stab 2000, 70, 485.
38. Nishida, H.; Yamashita, M.; Endoc, T. Polym Degrad Stab 2002, 78, 129.
39. Du, M. L.; Guo B. C.; Jia D. M. Eur Polym J 2006, 42, 1362.
40. Manitiu, M.; Horsch, S.; Gulari, E.; Kannan, R. M. Polymer 2009, 50, 3786.
41. Shelley, J. S.; Mather, P. T.; DeVries, K. L. Polymer 2001, 42, 5849.
42. Lee, C. J. Polym Eng Sci 1987, 27, 1015.
43. Liu, T. X.; Lim, K. P.; Tjiu, W. C.; Pramoda, K. P.; Chen, Z. K. Polymer 2003, 44, 3529.
44. Franchini, E.; Galy, J.; Gérard, J. F. J Colloid Interface Sci 2009, 329, 38.
45. Friedrich, K.; Fakirov, S.; Zhang, Z. Polymer Composites: From Nano-to-Macro-Scale; Springer: New York, 2005, p 16.